

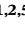

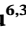




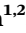






RESEARCH ARTICLE

10.1029/2018JD029489

Inversion Estimates of Lognormally Distributed Methane Emission Rates From the Haynesville-Bossier Oil and Gas Production Region Using Airborne Measurements

Yu Yan Cui^{1,2,3} , Daven K. Henze⁴ , Jerome Brioude^{1,2,5} , Wayne M. Angevine^{1,2} , Zhen Liu^{6,3} , Nicolas Bousserrez⁴ , Jonathan Guerrette^{1,2} , Stuart A. McKeen^{1,2} , Jeff Peischl^{1,2} , Bin Yuan^{1,2} , Thomas Ryerson² , Gregory Frost² , and Michael Trainer² 

¹Cooperative Institute for Research in Environmental Sciences, University of Colorado Boulder, Boulder, CO, USA,

²Chemical Sciences Division, Earth System Research Laboratory, NOAA, Boulder, CO, USA, ³Now at California Air

Resources Board, Sacramento, CA, USA, ⁴Department of Mechanical Engineering, University of Colorado Boulder,

Boulder, CO, USA, ⁵Laboratoire de l'Atmosphère et des Cyclones, UMR8105, CNRS-Meteo France-Universite La Reunion,

La Reunion, France, ⁶Ramboll Environ US Corporation, Novato, CA, USA

Key Points:

- A set of inversion calculations provide estimates of lognormally distributed methane emissions that are confirmed by two other top-down methods
- Multiple meteorological configurations and inversion approaches are used to capture transport errors and inversion biases
- The best estimate from our inversions shows that CH₄ emissions are likely underestimated by an EPA inventory for this oil and natural gas basin

Supporting Information:

- Supporting Information S1

Correspondence to:

Y. Y. Cui,
yuyan.cui@noaa.gov

Citation:

Cui, Y. Y., Henze, D. K., Brioude, J., Angevine, W. M., Liu, Z., Bousserrez, N., et al. (2019). Inversion estimates of lognormally distributed methane emission rates from the Haynesville-Bossier oil and gas production region using airborne measurements. *Journal of Geophysical Research: Atmospheres*, 124, 3520–3531. <https://doi.org/10.1029/2018JD029489>

Received 14 AUG 2018

Accepted 5 FEB 2019

Accepted article online 15 FEB 2019

Published online 18 MAR 2019

Abstract Quantifying methane (CH₄) emissions from the oil and natural gas (O/NG) production sector is an important regulatory challenge in the United States. In this study, we conduct a set of inversion calculations using different methods to quantify lognormal distributed CH₄ surface fluxes in the Haynesville-Bossier O/NG production basin in Texas and Louisiana, combining three statistical cost functions, four meteorological configurations, and two days of aircraft measurements from a 2013 field campaign. We aggregate our posterior flux estimates to derive our best estimate of the basin-wide CH₄ emissions, 76 metric tons/hr, with a 95% highest density interval of 51–104 metric tons/hr, in agreement with previous estimates using mass balance and eddy covariance approaches with the same aircraft measurements. Our inversion estimate of basin-wide CH₄ emissions is 133% (89%–182%, 95% highest density interval) of a gridded Environmental Protection Agency's inventory for 2012, and the largest discrepancies between our study and this inventory are located in the northeastern quadrant of the basin containing active unconventional O/NG wells. Our inversion approach provides a new spatiotemporal characterization of CH₄ emissions in this O/NG production region and shows the usefulness of inverse modeling for improving O/NG CH₄ emission estimates.

Plain Language Summary Oil and natural gas (O/NG)-related methane (CH₄) emission estimates have drawn great concern because activity in this industry has increased dramatically over the past decade. However, estimating CH₄ emissions from O/NG production regions is very challenging because the emission rates are highly heterogeneous. To properly characterize the CH₄ emissions in the Haynesville oil and gas production region, we develop an inverse modeling system to handle different ways of characterizing the highly skewed (i.e., lognormally distributed) CH₄ sources in Haynesville. The inverse model calculations are driven by high-frequency, high-precision CH₄ mixing ratios measured on a National Oceanic and Atmospheric Administration aircraft during a field study in the summer of 2013. We use a variety of meteorological simulations to define the transport errors in our inversions, and we take advantage of a resampling method to characterize the posterior uncertainties. Our results suggest that Haynesville's CH₄ emissions are likely underestimated in the U.S. Environmental Protection Agency's national CH₄ inventory and particularly in the subdomain where many active unconventional wells are located; day-to-day variability in Haynesville's overall CH₄ emissions likely exists. Our work offers an extensive characterization of inversions' uncertainties and demonstrate the feasibility of improving CH₄ emission estimates from O/NG production regions using high quality aircraft observations.

1. Introduction

Methane (CH₄) is a potent greenhouse gas (GHG) with a large global warming potential. It also impacts atmospheric oxidants by modulating global hydroxyl radical levels and the production of tropospheric ozone. Reducing CH₄ emissions is a part of GHG mitigation strategies in the United States and Europe (United Nations Framework Convention on Climate Change, 2016). Effective regulations for achieving GHG mitigation targets require quantification of CH₄ emissions from specific source sectors.

©2019. The Authors.

This is an open access article under the terms of the Creative Commons Attribution-NonCommercial-NoDerivs License, which permits use and distribution in any medium, provided the original work is properly cited, the use is non-commercial and no modifications or adaptations are made.

Over the past decade, oil and natural gas (O/NG) production has increased significantly in the United States (Energy Information Administration, 2017). The emission rate of CH₄ from leaks and other fugitive sources during O/NG production, expressed as a percentage of the natural gas produced, is estimated at 0.3–8.9% across U.S. basins (e.g., Karion et al., 2013; Peischl et al., 2015). This wide range in CH₄ leak rates in turn leads to uncertainty in the net climate impacts of replacing coal with natural gas as a fuel source (Alvarez et al., 2012, 2018). Quantifying CH₄ emission rates from the O/NG production sector is therefore an active area of scientific inquiry (Miller & Michalak, 2017).

Conventional component/facility-based inventories using average emission factors for each known source category by an aggregated or annualized activity factor face challenges in characterizing CH₄ emissions from O/NG production, because of the large spatial and temporal variability in activity profiles and emission factors for the various processes involved (e.g., Lan et al., 2015). CH₄ sources in O/NG production basins may have time-varying leakage rates (e.g., Vaughn et al., 2018), and there can be a number of “super emitting” sources that account for a large fraction of the emissions (e.g., Brandt et al., 2016) and missed sources caused by abnormal operating conditions (Alvarez et al., 2018). These complications make it difficult to obtain robust basin-wide CH₄ emission estimates and subsequently extrapolate emissions from this sector to regional and national scales. New bottom-up emission models (Alvarez et al., 2018) have been developed using recently reported facility-scale measurements specific to each segment; nevertheless, such models highly demand extensive facility-level measurements, and nonlinear statistical calculations may be not easy to extend to other regions where there is lack of detailed measurements.

On the other hand, numerous recent top-down (i.e., relying on atmospheric observations and modeling) efforts have focused on quantifying CH₄ emission rates in U.S. O/NG basins and developing emission factors for this specific source sector, in order to promote better understanding of regional-, national-, and global-scale budgets of CH₄ and its associated climate and tropospheric oxidant impacts (e.g., Alvarez et al., 2018; Houweling et al., 2017; Jeong et al., 2016; Karion et al., 2013; Kort et al., 2014; Miller et al., 2013; Pétron et al., 2012; Schwietzke et al., 2017; Sheng et al., 2018; Turner et al., 2015; Wecht et al., 2014). The comparisons between top-down and bottom-up estimates improve our accurate estimating emissions.

One such top-down effort is the aircraft measurement. Atmospheric measurements of CH₄ mixing ratios from the aircraft provide the basis of several top-down approaches to constrain basin-wide CH₄ emissions for the O/NG basins, such as the mass balance method (e.g., Alvarez et al., 2018), the eddy covariance flux approach (e.g., Yuan et al., 2015), and inverse modeling estimates (e.g., Sheng et al., 2018). The comparisons of these independent methods can reduce the uncertainty in top-down constraining CH₄ emission for the O/NG production sector. The mass balance method as a measurement-based top-down approach has been used widely to constrain basin-wide CH₄ emissions for the O/NG basins using aircraft measurements (e.g., Alvarez et al., 2018). The mass balance approach typically can quantify domain-wide emissions with high confidence. However, it is only feasible under highly favorable meteorological conditions over certain geographic topography, limiting its application for measurements from all flight days to identify and constrain the temporal variability in emissions. For example, only two out of the 15 research flights in a 2015 study in the Fayetteville oil and gas production region were suitable for performing mass balance estimates of CH₄ emissions (Schwietzke et al., 2017). Complex meteorological conditions, for example, the Fresno eddy circulation in the San Joaquin Valley in California, often impede this measurement-based estimate (Cui et al., 2017) and can even result in large errors due to mischaracterized winds (Ren et al., 2018). Meanwhile, it is not suitable for identifying spatial patterns of emitters in the O/NG domain. The eddy covariance flux method as an alternative measurement-based approach is less constrained by the meteorological conditions than the mass balance approach and derives the flux along or near the flight tracks to present the spatial patterns of emitters. However, one must extrapolate eddy covariance flux results from a small fraction of the investigated region in order to estimate a domain-wide emission rate, which may face challenging especially if the footprints along the flight track only represent a small fraction of the investigated region. The model-based inversion calculation can be an alternative approach to quantify CH₄ emissions from the O/NG basins that in principle can use all time-varying measurements collected by a research aircraft under different meteorological conditions. The model-based

approach could quantify CH₄ emissions for the O/NG basins including the information on the spatial patterns of the emitters as well as the temporal variation of emissions using measurements from different flights. However, inversion modeling has its own challenges, namely, quantifying the influence of uncertainties in the prior information, the model transport simulations, and the statistical estimation assumptions on the resulting posterior emissions estimates. An ensemble of inversions that test the sensitivities to these factors may be able to achieve more optimal emission estimates.

National Oceanic and Atmospheric Administration (NOAA) aircraft field campaign “Studying the Interactions between Natural and Anthropogenic Emissions at the Nexus of Climate Change and Air Quality” (SENEX) took place in the southeastern United States during the summer of 2013. The NOAA P-3 aircraft flew over the Haynesville-Bossier, Fayetteville-Western Arkoma, and northeastern Marcellus O/NG production regions during the campaign (Warneke et al., 2016). Mass balance and eddy covariance calculations have been used to quantify CH₄ emissions for the Haynesville-Bossier O/NG production region during SENEX (Peischl et al., 2015; Yuan et al., 2015). In this study, we develop the model-based inversion calculations to quantify total CH₄ emissions for the same domain together with the information on the spatial distribution of the emitters. The two previous measurements-based estimates provide cross-comparisons with our inversion results that reduce the uncertainty in constraining basin-wide emission rates. Moreover, beyond the two previous studies, here we use our spatially resolved posterior analysis to evaluate a recent gridded Environmental Protection Agency (EPA) GHG inventory for 2012 (Maasackers et al., 2016) and investigate the discrepancy between the prior and the posterior estimates of the spatial patterns of the emissions. Lastly, we consider day-to-day variations in the basin-wide CH₄ emissions.

The Haynesville-Bossier O/NG basin ($\sim 180 \times 133$ km²) in east Texas and northwest Louisiana is one of the most productive O/NG basins in the United States and had the largest natural gas production among the three basins targeted during SENEX. Yuan et al. (2015) showed that CH₄ emissions in the Haynesville-Bossier O/NG production are lognormally distributed, which is consistent with previous studies that the distribution of CH₄ emitters is typically highly skewed in O/NG production basins (e.g., Brandt et al., 2016). Meanwhile, we find the distribution of the observed CH₄ enhancements from the aircraft measurements is closer to lognormal than to Gaussian. Conventional inversion frameworks that assume a normal distribution of CH₄ surface fluxes (and most commonly normal distributed observation-model residuals as well) likely lead to suboptimal posterior estimates for the O/NG production sector. To our knowledge, although lognormal inversion has not been applied for estimating emissions from the O/NG production basins to date, the theoretical framework is developed by previous authors. The lognormal assumption for the state variables have been made in previous inversions to estimate positive definite state variables (e.g., Brioude et al., 2011; Guerrette & Henze, 2017; Wecht et al., 2014). Meanwhile, data assimilation methods for lognormal distributed observations (and hence observational errors, as argued by Fletcher and Zupanski, 2006) have been developed for meteorological variables. Bocquet et al. (2010) introduced an inversion framework with lognormal statistics in both state and observation spaces while assuming errors to be of multiplicative nature. Such a framework has been applied in inversion analysis of aerosol size distributions and fire smoke emissions (Saide et al., 2012, 2015). In this work, we continue to develop our inversion system (Brioude et al., 2011; Cui et al., 2015, 2017) within the lognormal framework for both the observation and state spaces assuming errors to be of multiplicative nature and apply the system to seek top-down estimate of CH₄ emissions for an O/NG production basin. We conduct an ensemble of inversions by using multiple meteorological configurations and varying the cost function to solve for all three commonly used estimators (the mode, median, and mean) for the state variable (CH₄ emission), followed by a resampling procedure to yield uncertainty estimates for the optimal solutions. We use such an ensemble approach to comprehensively assess uncertainties stemming from meteorological and transport modeling, as well as those associated with the statistical estimator from different cost function used by the inversion. This comprehensive inversion analysis in the lognormal framework could be used to inform and improve future inversion studies for specific sectors with a fat-tailed distribution profile.

The details of our methodology are described in section 2. Our optimized emissions and interpretation of the results are presented in section 3. Conclusions are given in section 4.

2. Methodology

2.1. Aircraft Measurements and the Prior Inventory

During the SENEX field campaign, the NOAA P-3 aircraft flew over Haynesville-Bossier on 10 and 25 June 2013. CH₄ mixing ratios were sampled every second along the aircraft flight tracks (Peischl et al., 2012). All of the measurements were sampled during the late morning to early afternoon, and ~90% of measurements were taken at altitudes below 1,500 m above ground level (agl; see Figure S1 and Text S1 in the supporting information). On 10 June, skies were clear. The average wind speed measured aboard the P-3 was 3.2 ± 0.9 m/s. Winds were from the south in the southern part of Haynesville and then shifted to westerly in the northern portion of the region. Based on available vertical profiles of potential temperatures from the flight measurements, the planetary boundary layer (PBL) height increased from ~1,000 to ~1,500 m agl during the measurement time in Haynesville. On 25 June, the winds were consistently from the south southwest throughout the study area at 6.4 ± 1.2 m/s. It was cloudy that day, and the PBL height increased from ~1,500 to ~2,000 m agl during the time of the flight.

The tracks of the two flights are shown in Figure 1, colored by the observed CH₄ mixing ratios. The magnitudes and spatial patterns of CH₄ mixing ratios measured during the two flights, which followed similar tracks, were quite different. We largely attribute these differences to the different coherent PBL structures on the two days. The PBL height on 10 June was lower than the PBL height on 25 June, and as a result, the 10 June flight sampled higher CH₄ mixing ratios. Day-to-day variability of CH₄ emissions, demonstrated in other O/NG production basins (Allen et al., 2017; Lavoie et al., 2017; Schwietzke et al., 2017), may also contribute to the variations of CH₄ mixing ratios between the two days.

For the 10 June flight, the changing wind direction made it challenging to conduct a mass balance estimate of CH₄ emissions. Therefore, Peischl et al. (2015) used only observations collected from the 25 June flight to conduct a mass balance estimate of CH₄ emissions in the region. In this study, we use both of the flights to conduct our inversion estimates. For each, we use 120-s averaged CH₄ measurements below 1,500 m agl in the domain. The initial background CH₄ mixing ratio for the 25 June flight ($1,847 \pm 3$ ppbv) was determined by Peischl et al. (2015) based on measurements collected during upwind transects. In our study, we also use this method to determine the background CH₄ for the 10 June flight, which we estimate to be $1,905 \pm 20$ ppbv. For details of the background calculation, refer to Figure S2 and Text S1 in the supporting information. The CH₄ mixing ratio enhancements after subtracting the background concentration are used in the inverse modeling system.

The monthly (June) gridded CH₄ emission inventory from Maasackers et al. (2016) is used as the initial emissions estimate (Figure 1). This inventory distributes the U.S. EPA's Greenhouse Gas Inventory for 2012 at $0.1^\circ \times 0.1^\circ$ spatial resolution.

2.2. Atmospheric Transport Models

We use the FLEXPART-WRF mesoscale Lagrangian model (Brioude et al., 2013) to simulate atmospheric transport. For each flight, 10,000 particles are released at the locations (Figure 1) of the 120-s averaged measurements along the flight tracks. FLEXPART simulates their back trajectories over 5 days (Figure 2). We use each of the back trajectories to conduct the inverse modeling analysis. More details of the FLEXPART-WRF configuration can be found in Cui et al. (2015).

The WRF simulations driving FLEXPART are obtained from Angevine et al. (2014), who used six different WRF configurations to estimate the uncertainty of FLEXPART transport simulations over the southeastern United States. We use four (Table 1) of the six simulations from Angevine et al. (2014), including combinations of different global meteorological model initializations (U.S. GFS and European ERA-interim), PBL schemes (the Mellor-Yamada-Nakanishi-Niino level 2.5 (MYNN) scheme (Nakanishi & Niino, 2009) and the Total Energy-Mass Flux (TEMF) scheme (Angevine et al., 2010), and a cumulus cloud formation scheme (G3D; Grell & Devenyi, 2002) with or without treatment of shallow convection. Two other WRF configurations from Angevine et al. (2014) with additional soil moisture treatments have similar performance in simulating CH₄ mixing ratios compared with the WRF simulations without soil moisture treatments, so we did not use them in this study.

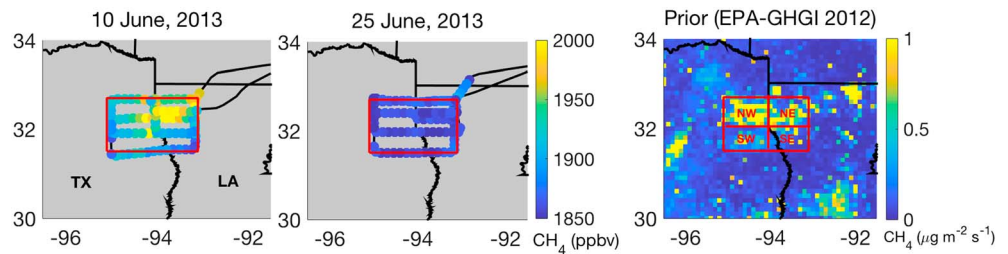


Figure 1. The left and middle panels show 120-s averages of CH₄ mixing ratios below 1,500 m above ground level sampled by the National Oceanic and Atmospheric Administration P-3 flights on 10 June and 25 June 2013 during Studying the Interactions between Natural and Anthropogenic Emissions at the Nexus of Climate Change and Air Quality. Five-day back trajectories are simulated at the locations of each of the average measurements shown here. The right panel shows the prior CH₄ inventory at 0.1 × 0.1° spatial resolution from the work of Maasackers et al. (2016). We divided the domain into four quadrants (“NE,” “SE,” “SW,” and “NW”) to study the spatial patterns of CH₄ emissions.

We evaluate four WRF 12-km simulations by comparing them to 120-s average observations of wind speed, wind direction, and planetary boundary layer height (PBLH) measured along the flight tracks (Figure 3). Both wind speed and wind direction errors are small in the four WRF simulations in terms of the interquartile range, and we found that the mean relative errors between observed and simulated wind speeds and directions are within 22%. The errors in simulated PBLHs are within 50% for the 10 and 25 June flights, respectively. The four WRF configurations systematically overestimate wind speeds in the simulations for the 25 June flight. Also, the PBLHs in the WRF4 run for 10 June are systematically high. High biases in the modeled wind speed or PBLHs could theoretically result in the sensitivities of the measurements to the surface fluxes being underestimated, which in turn would cause overestimated emission rates from the inversions if the simulations are otherwise perfect. In this study, we conduct our inversion calculations assuming no systematic biases in model transport, based on the limited aircraft observations available to us. Based on the systematic biases noted above, overestimates of emission rates in the inversions for the 25 June flight and with the WRF4 simulation for 10 June flight are possible. In our study, we assume meteorological uncertainty is the largest contributor to the uncertainty of the atmospheric transport simulation (Hegarty et al., 2013). Based on a conservative evaluation of the wind fields and PBLHs, we assign a 50% relative uncertainty to the measurement enhancements to present the transport model in the inversions for both the 10 and 25 June flights.

2.3. Inverse Modeling Framework

In this study, we continue to develop our mesoscale Bayesian inverse modeling system to quantify CH₄ emissions for the O/NG production basin based on SENEX aircraft measurements. This system has been used to

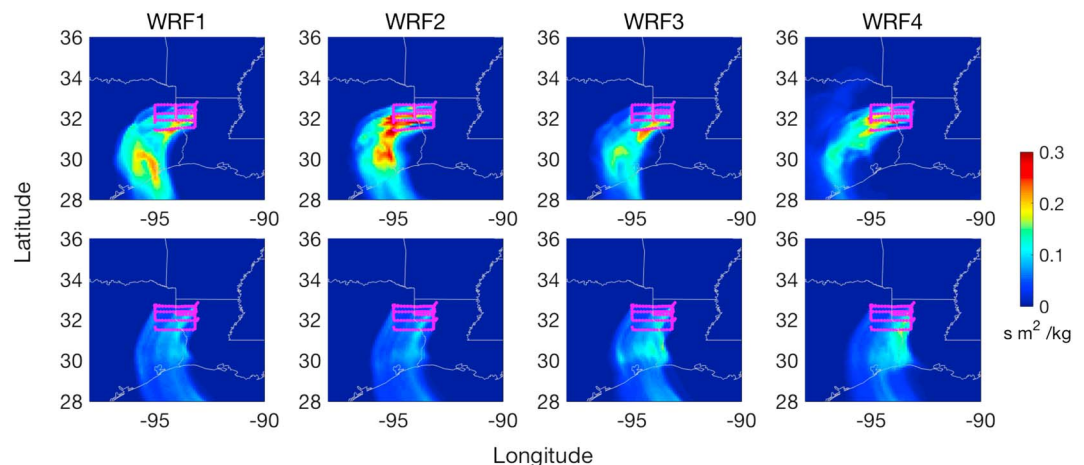


Figure 2. The averaged footprints from FLEXPART driven by four different WRF simulations for the 10 June (top row) and 25 June (bottom row) flights.

Table 1
Names and Primary Configurations of Four WRF Runs Used in This Study

	Grid	Initialization	PBL	Cumulus
WRF1	12 km	GFS	MYNN level 2.5	G3D with shallow
WRF2	12 km	ERA-interim	MYNN level 2.5	G3D with shallow
WRF3	12 km	GFS	TEMF	G3D no shallow
WRF4	12 km	ERA-interim	TEMF	G3D no shallow

Note. ERA = European Centre for Medium-Range Weather Forecasts Re-Analysis; PBL = planetary boundary layer; MYNN = Mellor-Yamada-Nakanishi-Niino; TEMF = Total Energy-Mass Flux.

estimate CH₄ emissions in California using aircraft measurements (Cui et al., 2015, 2017). We assume that concentration deviations above background values and emissions follow lognormal distributions associated with the errors (the model-observation mismatch and flux error) to be of multiplicative nature (Bocquet et al., 2010; Tian et al., 2013). The lognormal assumption is suitable and important for this study. We also assume that the aircraft measurements took place near the CH₄ source region, so that the uptake of CH₄ by soils is negligible, and the state variables (i.e., the emission fluxes) are positive definite. The lognormal assumption is suitable and important for this study.

In our previous studies, we only focused on median-based inversions of CH₄ emission estimates in regions with multiple source sectors. In this study, we extend our system to include mode- and mean-based inversions, in order to discuss the range of values from each of those metrics and to better characterize surface fluxes using the assumptions of a lognormal distribution. In this study, there are two modifications for the median-based inversions compared with our previous work (Cui et al., 2015, 2017): (1) we present the posterior uncertainty with a 95% confidence interval instead of a 68% confidence interval; and (2) we increase the number of perturbations from 100 to 1,000, to match the number we used for calculations in mode- and mean-based inversions; details are shown below.

Given the assumption of a lognormal distribution of sources, we consider three estimators that characterize the structure of the CH₄ surface flux distribution from this O/NG production basin: mode, median, and mean. The cost functions associated with the three estimators (mode, median, and mean) are (Fletcher, 2010), respectively,

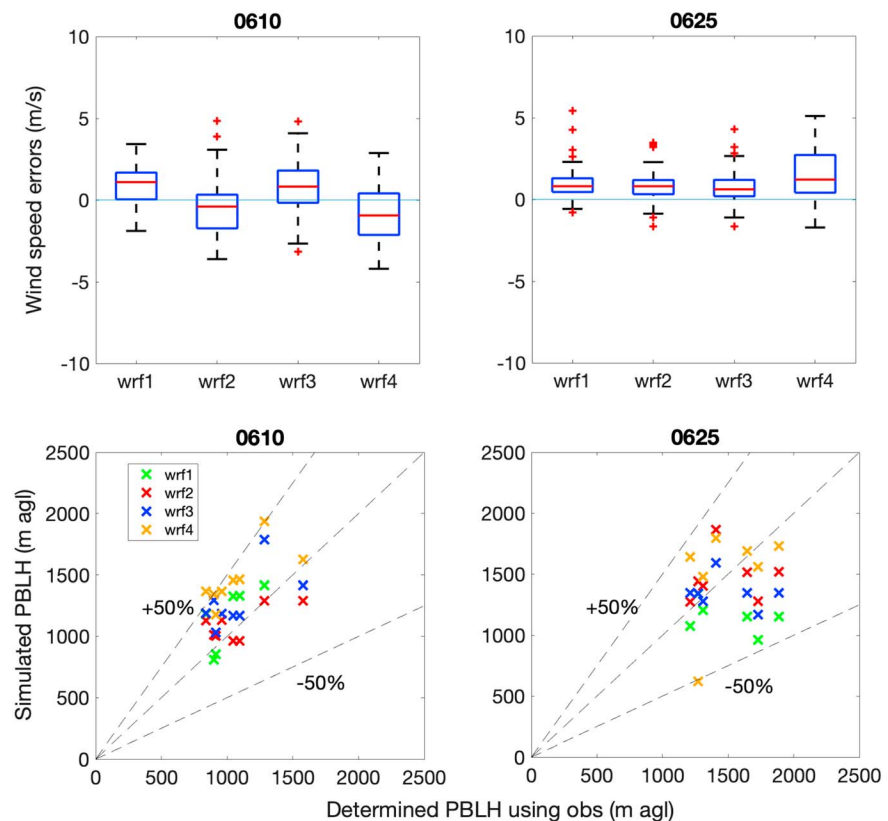


Figure 3. (top) Box plots showing the differences between the simulated and observed wind speeds and wind directions, using four different WRF configurations. (bottom) Scatter plots showing the PBLH determined from observations along the flight tracks (x axis) and the average PBLH simulated by WRF (y axis) in the same locations. The different color points represent different WRF configurations. The middle dotted line is the 1:1 line. PBLH = planetary boundary layer height.

$$J(x) = \frac{1}{2}(\ln(y_0) - \ln(Hx))^T (R^{-1}(\ln(y_0) - \ln(Hx)) + 2I_m) + \frac{1}{2}\alpha(\ln(x) - \ln(x_0))^T (B^{-1}(\ln(x) - \ln(x_0)) + 2I_n), \quad (1)$$

$$J(x) = \frac{1}{2}(\ln(y_0) - \ln(Hx))^T R^{-1}(\ln(y_0) - \ln(Hx)) + \frac{1}{2}\alpha(\ln(x) - \ln(x_0))^T B^{-1}(\ln(x) - \ln(x_0)), \quad (2)$$

$$J(x) = \frac{1}{2}(\ln(y_0) - \ln(Hx))^T (R^{-1}(\ln(y_0) - \ln(Hx)) - I_m) + \frac{1}{2}\alpha(\ln(x) - \ln(x_0))^T (B^{-1}(\ln(x) - \ln(x_0)) - I_n), \quad (3)$$

where \mathbf{y}_0 (dimension: $m \times 1$) is the measured time series of CH_4 mixing ratio enhancement above a defined background; \mathbf{H} (dimension: $m \times n$) is the source-receptor relationship matrix calculated by FLEXPART-WRF; \mathbf{R} (dimension: $m \times m$) and \mathbf{B} (dimension: $n \times n$) are the error covariance matrices of the model-observation mismatch and the prior emissions, respectively (\mathbf{R} and \mathbf{B} are assumed to be diagonal matrices); \mathbf{x}_0 (dimension: $n \times 1$) is the prior emission inventory; we adjust and optimize x (dimension: $n \times 1$) to derive the posterior emission inventory by minimizing the cost function; \mathbf{I}_m (dimension: $m \times m$) and \mathbf{I}_n (dimension: $n \times n$) are unit matrices of size m and n , respectively. Note that a unit matrix needs to be introduced into the cost functions for the mode and the mean but not the median during the logarithmic calculation; and α is a regularization parameter used to tune the balance between the contributions of model-observation errors and the constraints of the prior emission estimate errors (e.g., Hansen, 1998; Davoine & Bocquet, 2007; Henze et al., 2009; Saide et al., 2012). The descriptions of how we construct \mathbf{R} and \mathbf{B} and tune the value of α are in Text S1 in the supporting information. It is the first time to introduce equations (1) and (3) to our inverse modeling system in such inversion analysis.

In a Gaussian inverse modeling framework, it is possible to approximate posterior uncertainty from the inverse of the second derivative (Hessian) of the cost function. Such methods do not extend simply to the log-normal framework. Therefore, we use a resampling method to derive our final posterior emissions and the associated posterior uncertainties, to avoid the difficulty in deriving Hessian matrices for the mode, median, and mean inversions in the lognormal framework. Specifically, we construct an ensemble of 1,000 inversions by applying perturbed scaling factors to measurement enhancements and prior fluxes that are uniformly distributed random numbers in the interval (0.5, 1.5) and (0, 2), respectively which are assigned to match relative uncertainty assumptions used for \mathbf{R} and \mathbf{B} (Text S1). We consider the given perturbation ranges to be the fair and conservative ranges in the study. To discuss the robustness of the results due to the choice of perturbation intervals, we also conduct another set of ensemble runs that use a smaller perturbation range ((0.3 1.3) and (0.5 1.5) for \mathbf{R} and \mathbf{B} , respectively) to illustrate what a more “optimistic” estimate could be in the Text S1. The two setups derive the similar results, and here we present the analysis (section 3) based on the conservative analysis. In each inversion sample, we obtain the basin-wide total CH_4 emission estimates by summing optimized values for individual grids in the domain. Consequently, results from 1,000 inversions form a distribution of the posterior basin-wide estimates, from which the mode value of a histogram is considered the final posterior basin-wide estimate and the 95% highest posterior density interval (HDI) is considered as the associated posterior uncertainty range (Fischer et al., 2018; Hyndman, 1996). An example of an aggregated basin-wide estimate based on 1,000 inversions is shown in Figure 4a. This same method of assigning a distribution to a set of samples is used to aggregate basin-wide total CH_4 emission estimate, such as combining inversions from multiple meteorological configuration and inversion cost functions in Figure 4b.

3. Results and Discussion

3.1. Estimates of Total CH_4 Emissions

Here we present our model-based inversion analysis using the aircraft measurements on two different days to characterize the CH_4 surface flux spatial distributions and basin-wide emissions in the Haynesville-Bossier O/NG production region. We find that the simulated CH_4 mixing ratios using the posterior

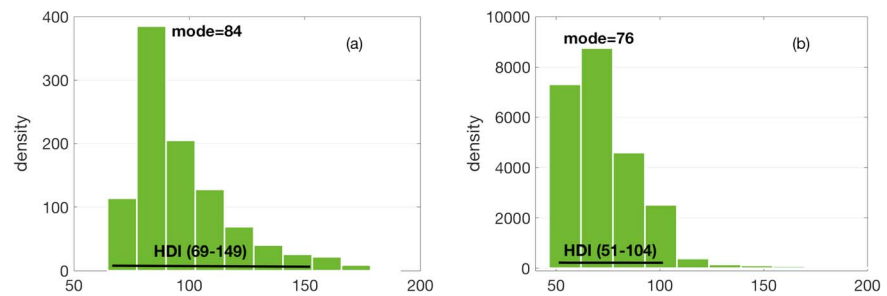


Figure 4. (a) The density distribution of posterior estimates derived by WRF1 and equation (3), as an example of the results of our inversion calculations. (b) The density distribution combining a variety of inversions using four typical sets of meteorological simulations, three optimal algorithms, and observed data from two flights, from which our final domain-wide estimate is obtained. In the study, we use the mode value of the density distribution to represent the final posterior estimate of the domain-wide CH₄ emissions, and the associated uncertainties are represented by a 95% highest posterior density interval (HDI).

emission estimates have a higher coefficient of determination (r^2) and lower mean biases versus the measured CH₄ mixing ratios, in comparison with the simulations using the prior inventory (see Figure S4 in the supporting information), which demonstrates that the inversion framework is working as expected.

While the inverse modeling framework provides emissions estimates in each model grid cell throughout the entire domain, the aircraft measurements are too sparse to completely constrain each of these values independently. Thus, to quantify the information about emissions constrained by the airborne concentration measurements within the inverse modeling system, we compute maps of the diagonal of the Fisher information matrix (Cui et al., 2015) for each flight (Figure 5 and supporting information Figure S5). The regions associated with high values of the Fisher information matrix represent the areas of the domain that are well constrained by the observations. Comparing Figure 5 (or Figure S5) to Figure 1, we see that the measurements on both days are capable of constraining the emissions throughout the Haynesville region, especially in the northern part of the domain where most of the sources are located (more information of individual sources in the domain refer to Table S1 and Figure S7 in the supporting information).

The various estimates of basin-wide CH₄ emissions, derived from aggregating our posterior estimates of CH₄ surface fluxes in the domain in different ways, are shown in Figure 6. Inversions for each flight for both days with each transport simulation and each optimization algorithm are shown in Figure 6a. We combine inversion analyses of the four transport simulation cases to obtain inversions for each day for the posterior mode, median, and mean (Figure 6b). The differences among center point values of the solutions in the mode, median, and mean characterize a skewed distribution of the basin-wide CH₄ emissions. The comprehensive inversion estimates in this work provide a new way to characterize CH₄ emission rates for an O/NG production basin that allows for such non-Gaussian behavior.

To better constrain the lognormal distributed emissions, we combine the range of three solutions of the mode, median and mean to derive the basin-wide total CH₄ emissions to be 79 (55–107 at 95% HDI) on 10

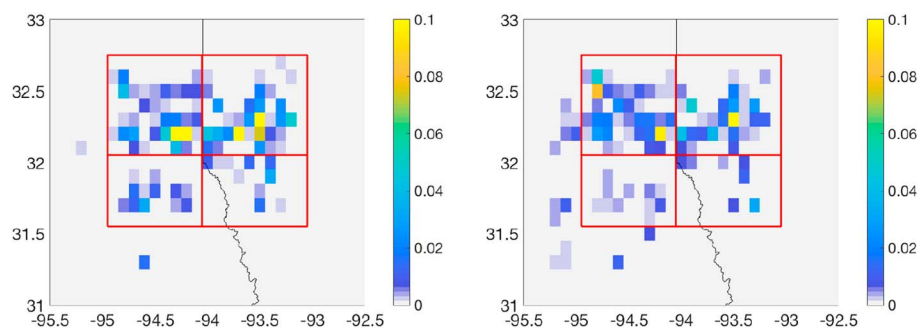


Figure 5. The maps represent the Fisher information matrix weighted by the maximum value of the matrix, at a spatial resolution of $0.1 \times 0.1^\circ$. Here examples are based on the WRF1 transport models (results from the other three meteorological model configurations are shown in Figure S5).

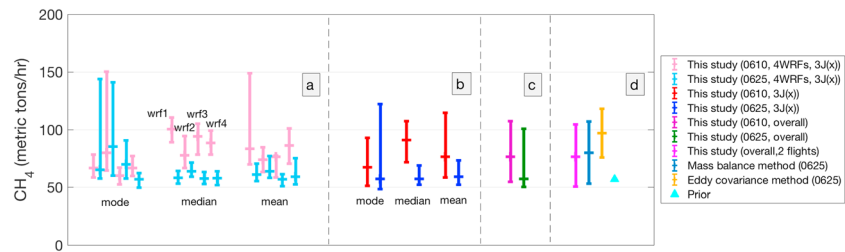


Figure 6. Comprehensive estimates of domain-wide CH₄ emissions in the Haynesville oil and gas production region: (a) inversions from each of the four meteorological configurations and each of the three optimized statistical measures for the two flights; (b) combined inversions of the four meteorological configurations for the two flights; (c) combined inversions of the four meteorological configurations and three statistical measures for the two flights; and (d) the comparisons of overall posterior estimates combining all of our inversions (Figure 3), the previous top-down studies, and the prior estimates in the same domain.

June and 57 (50–101 at 95% HDI) on 25 June (Figure 6c) respectively. Although the center point estimates on 10 June appear higher than those on 25 June, which may suggest a possible day-to-day variability in the basin-wide emissions, the large associated uncertainties degrade the statistical significance of this difference. The magnitude of the variability is comparable to a day-to-day variability noted in previous studies in the Fayetteville O/NG basin (Schwietzke et al., 2017). Further measurements beyond this aircraft campaign evaluated in the work are required to fully investigate the temporal variability of emissions in the basin (Vaughn et al., 2018).

When we combine inversions for both flights based on multiple transport models for each inverse modeling formulation, we derive a total CH₄ emission of 76 metric tons/hr in the Haynesville-Bossier O/NG drilling region. Our lower and upper bound uncertainties are 51 and 104 metric tons/hr, based on the posterior's 95% HDI (Figures 6d and 4). In comparison (Figure 6d), the prior inventory from Maasackers et al. (2016), which is based on EPA's 2012 Greenhouse Gas Inventory, has a domain-wide emission of 57 metric tons CH₄/hr, which falls within our top-down uncertainty range but is close to the lower bound (Figure 6d). Overall, our posterior estimates are 133% (89–182% at 95% HDI) of the bottom-up estimate from Maasackers et al. (2016).

3.2. Cross-Comparisons Among Three Top-Down Approaches

Peischl et al. (2015) used the mass balance approach to obtain a total emission of 80 ± 27 metric tons CH₄/hr in the same Haynesville-Bossier O/NG drilling domain for 25 June. Yuan et al. (2015) used the eddy covariance method to estimate emissions of 97 ± 21 metric tons CH₄/hr in the same domain on 25 June (Figure 6d). Both of the previous two studies reported problems in estimating emissions for 10 June, so that estimates of day-to-day emission variability using these other top-down methods could not be made. Our estimates and these previous studies are comparable in magnitude. Inversion results for 25 June in our study are smaller than the mass balance estimates, while the estimates from the eddy covariance method are some-

what higher than the mass balance estimate. In general, the three top-down estimates are consistent with one another within the estimated uncertainties.

3.3. The Spatial Pattern of CH₄ Emissions

Our inverse modeling approach allows for a top-down characterization of the spatial distribution of CH₄ emissions in the Haynesville-Bossier O/NG drilling region. The optimized spatial patterns of CH₄ emissions help to identify the locations of high emissions and may provide a guide to O/NG regulators.

The limited number of measurements from these flights may not be sufficient to constrain the emissions in each model grid cell of the domain (see section 3.1). So we divide the Haynesville region into four quadrants (Figure 1) based on the distribution of wells (see Figure 3 of Peischl et al., 2015) and the border between Texas and Louisiana. Figure 7 shows the

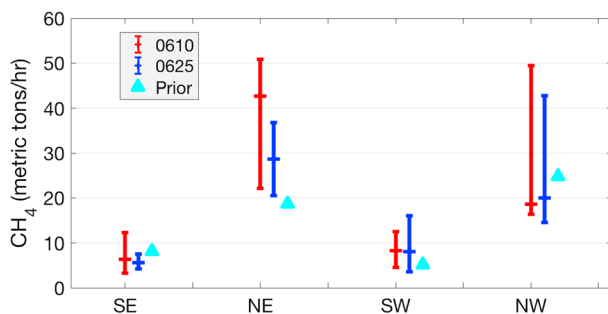


Figure 7. Posterior emission estimates of CH₄ for the four Haynesville quadrants shown in Figure 1. Emission estimates and associated uncertainties shown here are ensemble values of four meteorological configurations and three optimized statistical measures.

prior and the constrained emission estimates of CH₄ from all inversions for the four quadrants of the domain for each flight. The northern part of the domain contributes 76% of total basin-wide CH₄ emissions in the prior inventory. This part of the domain is associated with high values of the Fisher information matrix (Figure 5) and is therefore well constrained by our inversions. The northwestern quadrant contains many active conventional and unconventional gas wells and is the largest emitting area (25 metric tons/hr) in the prior inventory. Our inversions for the northwestern quadrant on both 10 and 25 June estimate somewhat lower emission rates than the prior estimate, with center point values of the inversions 20–24% lower than the prior.

The northeastern quadrant has most of the active unconventional gas wells and is the second highest emitting part of the basin according to the prior estimate. However, we estimate that the northeastern quadrant has the highest CH₄ emissions in the domain using our inverse modeling based on the aircraft measurements. The northeastern quadrant shows the largest differences in emissions between the two flight days, as well as the largest departure of the posterior value from prior emission estimate. In the northeastern quadrant, our inversions for the 10 and 25 June flights yield 42 (95% HDI: 22–51) and 28 (95% HDI: 21–37) metric tons CH₄/hr, respectively. Our posterior values are higher than the prior (19 metric tons/hr) by factors of 1.5–2.2 for the center point values, although the large associated uncertainties degrade the statistical significance of these differences. In the Haynesville-Bossier area, Peischl et al. (2015) estimated that other sources, such as livestock, point sources, and coal mines, contribute a relatively small fraction of the total basin-wide CH₄ emissions in the domain. Based on our inversion analysis, we suggest that future work could focus on better quantifying CH₄ emissions from unconventional wells in the northeastern quadrant of the domain, together with CH₄ emissions from the city of Shreveport, Louisiana, which is also located in that quadrant.

4. Conclusions

O/NG production is a major sector of U.S. CH₄ emissions, contributing the largest fraction of CH₄ emissions from the O/NG industry. Targeting CH₄ emissions for reductions requires accurate accounting of the contributions from this sector. In the summer of 2013, a NOAA aircraft participating in the SENEX field campaign flew over the Haynesville-Bossier O/NG production basin on two different days along similar east-west flight paths. Peischl et al. (2015) and Yuan et al. (2015) previously used the mass balance and eddy covariance techniques, respectively, to quantify total CH₄ emissions for this basin using these aircraft measurements. In this study, we use the same aircraft measurements in an alternative model-based inverse method over the same domain to quantify the CH₄ emission fluxes and investigate the spatial and temporal variability in the emissions. We employ multiple transport models, solving for the median, mean, and mode with lognormal-based cost functions and use a resampling uncertainty quantification approach.

We estimate that the Haynesville-Bossier basin's CH₄ emission is 76 metric tons/hr, with a 95% probability of falling in the range of 51–104 metric tons/hr. Our estimate corresponds to 133% (89–182%) of a bottom-up estimate based on a gridded 2012 U.S. EPA GHG inventory (Maasackers et al., 2016). Our comprehensive inversion analysis relies on non-Gaussian posterior distributions that represent CH₄ emissions from O/NG production involving “super emitters” or abnormal operating conditions.

We find a variation between two days of CH₄ emissions in the Haynesville-Bossier O/NG production basin, which is within the uncertainties associated with the inversion calculations and therefore not significant. More measurements are necessary in the future to fully characterize temporal variation of emissions in this basin.

Based on our spatially resolved inversion results, we find the largest discrepancy between our analysis and the prior inventory is in the northeastern quadrant of the Haynesville basin, associated with a high density of unconventional wells; the posterior emission is a factor of 1.5–2.2 higher than the prior estimate in this quadrant.

Overall, our study demonstrates the importance and feasibility of uncertainty characterization of O/NG production emissions using aircraft observations and a comprehensive inversion analysis, which could be applied in future analyses.

Acknowledgments

The FLEXPART-WRF model is available at the official FLEXPART website (<http://flexpart.eu>). NOAA P-3 data are available and can be downloaded at the NOAA website (<https://esrl.noaa.gov/csd/groups/csd7/measurements/2013senex/P3/DataDownload/>). The lognormal Bayesian inverse software was developed at NOAA/ESRL/CSD and CIRES. We thank NOAA's High Performance Computing Program for their support in running FLEXPART-WRF. D. K. H. and N. B. acknowledge support from NOAA Climate Program Office (CPO; NA14OAR4310136) and NASA GEO-CAPE.

References

Allen, D. T., Cardoso-Saldana, F. J., & Kimura, Y. (2017). Variability in spatially and temporally resolved emissions and hydrocarbon source fingerprints for oil and gas sources in shale gas production regions. *Environmental Science & Technology*, *51*(20), 12,016–12,026. <https://doi.org/10.1021/acs.est.7b02202>

Alvarez, R. A., Pacala, S. W., Winebrake, J. J., Chameides, W. L., & Hamburg, S. P. (2012). Greater focus needed on methane leakage from natural gas infrastructure. *Proceedings of the National Academy of Sciences of the United States of America*, *109*(17), 6435–6440. <https://doi.org/10.1073/pnas.1202407109>

Alvarez, R. A., Zavala-Araiza, D., Lyon, D. R., Allen, D. T., Barkley, Z. R., Brandt, A. R., et al. (2018). Assessment of methane emissions from the U.S. oil and gas supply chain. *Science*, eaar7204. <https://doi.org/10.1126/science.aar7204>

Angevine, W. M., Brioude, J., McKeen, S., & Holloway, J. S. (2014). Uncertainty in Lagrangian pollutant transport simulations due to meteorological uncertainty at mesoscale. *Geoscientific Model Development*, *7*(6), 2817–2829. <https://doi.org/10.5194/gmd-7-2817-2014>

Angevine, W. M., Jiang, H., & Mauritsen, T. (2010). Performance of an eddy diffusivity–mass flux scheme for shallow cumulus boundary layers. *Monthly Weather Review*, *138*(7), 2895–2912. <https://doi.org/10.1175/2010MWR3142.1>

Bocquet, M., Pires, C. A., & Wu, L. (2010). Beyond Gaussian statistical modeling in geophysical data assimilation. *Monthly Weather Review*, *138*(8), 2997–3023. <https://doi.org/10.1175/2010MWR3164.1>

Brandt, A. R., Heath, G. A., & Cooley, D. (2016). Methane leaks from natural gas systems follow extreme distributions. *Environmental Science & Technology*, *50*(22), 12,512–12,520. <https://doi.org/10.1021/acs.est.6b04303>

Brioude, J., Arnold, D., Stohl, A., Cassiani, M., Morton, D., Seibert, P., et al. (2013). The Lagrangian particle dispersion model FLEXPART-WRF version 3.1. *Geoscientific Model Development*, *6*(6), 1889–1904. <https://doi.org/10.5194/gmd-6-1889-2013>

Brioude, J., Kim, S. W., Angevine, W. M., Frost, G. J., Lee, S. H., McKeen, S. A., et al. (2011). Top-down estimate of anthropogenic emission inventories and their interannual variability in Houston using a mesoscale inverse modeling technique. *Journal of Geophysical Research*, *116*, D20305. <https://doi.org/10.1029/2011JD016215>

Cui, Y. Y., Brioude, J., Angevine, W. M., Peischl, J., McKeen, S. A., Kim, S. W., et al. (2017). Top-down estimate of methane emissions in California using a mesoscale inverse modeling technique: The San Joaquin Valley. *Journal of Geophysical Research: Atmospheres*, *122*, 3686–3699. <https://doi.org/10.1002/2016JD026398>

Cui, Y. Y., Brioude, J., McKeen, S. A., Angevine, W. M., Kim, S. W., Frost, G. J., et al. (2015). Top-down estimate of methane emissions in California using a mesoscale inverse modeling technique: The South Coast Air Basin. *Journal of Geophysical Research: Atmospheres*, *120*, 6698–6711. <https://doi.org/10.1002/2014JD023002>

Davoine, X., & Bocquet, M. (2007). Inverse modelling-based reconstruction of the Chernobyl source term available for long-range transport. *Atmospheric Chemistry and Physics*, *7*(6), 1549–1564. <https://doi.org/10.5194/acp-7-1549-2007>

Energy Information Administration (2017). https://www.eia.gov/petroleum/wells/pdf/full_report.pdf

Fischer, M. L., Chan, W. R., Delp, W., Jeong, S., Rapp, V., & Zhu, Z. (2018). An estimate of natural gas methane emissions from California homes. *Environmental Science & Technology*, *52*(17), 10,205–10,213. <https://doi.org/10.1021/acs.est.8b03217>

Fletcher, S. J. (2010). Mixed Gaussian-lognormal four-dimensional data assimilation. *Tellus*, *62*(3), 266–287. <https://doi.org/10.1111/j.1600-0870.2010.00439.x>

Fletcher, S. J., & Zupanski, M. A. (2006). Data assimilation method for log-normally distributed observational errors. *Quarterly Journal of the Royal Meteorological Society*, *132*(621), 2505–2519. <https://doi.org/10.1256/qj.05.2222006>

Grell, G. A., & Devenyi, D. (2002). A generalized approach to parameterizing convection combining ensemble and data assimilation techniques. *Geophysical Research Letters*, *29*(14), 1693. <https://doi.org/10.1029/2002GL015311>

Guerrette, J. J., & Henze, D. K. (2017). Four-dimensional variational inversion of black carbon emissions during ARCTAS-CARB with WRFDA-Chem. *Atmospheric Chemistry and Physics*, *17*(12), 7605–7633. <https://doi.org/10.5194/acp-17-7605-2017>

Hansen, P. C. (1998). *Rank-deficient and discrete ill-posed problems: Numerical aspects of linear inversion*. Philadelphia, USA: SIAM. <https://doi.org/10.1137/1.9780898719697>

Hegarty, J., Draxler, R. R., Stein, A. F., Brioude, J., Mountain, M., Eluszkiewicz, J., et al. (2013). Evaluation of Lagrangian particle dispersion models with measurements from controlled tracer releases. *Journal of Applied Meteorology and Climatology*, *52*(12), 2623–2637. <https://doi.org/10.1175/JAMC-D-13-0125.1>

Henze, D. K., Seinfeld, J. H., & Shindell, D. T. (2009). Inverse modeling and mapping US air quality influences of inorganic PM_{2.5} precursor emissions using the adjoint of GEOS-Chem. *Atmospheric Chemistry and Physics*, *9*(16), 5877–5903. <https://doi.org/10.5194/acp-9-5877-2009>

Houweling, S., Bergamaschi, P., Chevallier, F., Heimann, M., Kaminski, T., Krol, M., et al. (2017). Global inverse modeling of CH₄ sources and sinks: An overview of methods. *Atmospheric Chemistry and Physics*, *17*(1), 235–256. <https://doi.org/10.5194/acp-17-235-2017>

Hyndman, R. J. (1996). Computing and graphing highest density regions. *The American Statistician*, *50*, 120–126.

Jeong, S., Newman, S., Zhang, J., Andrews, A. E., Bianco, L., Bagley, J., et al. (2016). Estimating methane emissions in California's urban and rural regions using multitower observations. *Journal of Geophysical Research: Atmospheres*, *121*, 13,031–13,049. <https://doi.org/10.1002/2016JD025404>

Karion, A., Sweeney, C., Pétron, G., Frost, G., Michael Hardesty, R., Kofler, J., et al. (2013). Methane emissions estimate from airborne measurements over a western United States natural gas field. *Geophysical Research Letters*, *40*, 4393–4397. <https://doi.org/10.1002/grl.50811>

Kort, E. A., Frankenberg, C., Costigan, K. R., Lindenmaier, R., Dubey, M. K., & Wunch, D. (2014). Four corners: The largest US methane anomaly viewed from space. *Geophysical Research Letters*, *41*, 6898–6903. <https://doi.org/10.1002/2014GL061503>

Lan, X., Talbot, R., Laine, P., & Torres, A. (2015). Characterizing fugitive methane emissions in the Barnett Shale area using a mobile laboratory. *Environmental Science & Technology*, *49*(13), 8139–8146. <https://doi.org/10.1021/es5063055>

Lavoie, T. N., Shepson, P. B., Cambaliza, M. O. L., Stirn, B. H., Conley, S., Mehrotra, S., et al. (2017). Spatiotemporal variability of methane emissions at oil and natural gas operations in the Eagle Ford Basin. *Environmental Science & Technology*, *51*(14), 8001–8009. <https://doi.org/10.1021/acs.est.7b00814>

Maasakkers, J. D., Jacob, D. J., Sulprizio, M. P., Turner, A. J., Weitz, M., Wirth, T., et al. (2016). Gridded national inventory of US methane emissions. *Environmental Science & Technology*, *50*(23), 13,123–13,133. <https://doi.org/10.1021/acs.est.6b02878>

Miller, S. M., & Michalak, A. M. (2017). Constraining sector-specific CO₂ and CH₄ emissions in the US. *Atmospheric Chemistry and Physics*, *17*(6), 3963–3985. <https://doi.org/10.5194/acp-17-3963-2017>

Miller, S. M., Wofsy, S. C., Michalak, A. M., Kort, E. A., Andrews, A. E., Biraud, S. C., et al. (2013). Anthropogenic emissions of methane in the United States. *Proceedings of the National Academy of Sciences of the United States of America*, *110*(50), 20,018–20,022. <https://doi.org/10.1073/pnas.1314392110>

- Nakanishi, M., & Niino, H. (2009). Development of an improved turbulence closure model for the atmospheric boundary layer. *Journal of the Meteorological Society of Japan*, 20(4), 851–912. <https://doi.org/10.1029/RG020i004p00851>
- Peischl, J., Ryerson, T. B., Aikin, K. C., de Gouw, J. A., Gilman, J. B., Holloway, J. S., et al. (2015). Quantifying atmospheric methane emissions from the Haynesville, Fayetteville, and northeastern Marcellus shale gas production regions. *Journal of Geophysical Research: Atmospheres*, 120, 2119–2139. <https://doi.org/10.1002/2014JD022697>
- Peischl, J., Ryerson, T. B., Holloway, J. S., Trainer, M., Andrews, A. E., Atlas, E. L., et al. (2012). Airborne observations of methane emissions from rice cultivation in the Sacramento Valley of California. *Journal of Geophysical Research*, 117, D00V25. <https://doi.org/10.1029/2012JD017994>
- Pétron, G., Frost, G., Miller, B. R., Hirsch, A. I., Montzka, S. A., Karion, A., et al. (2012). Hydrocarbon emissions characterization in the Colorado Front Range: A pilot study. *Journal of Geophysical Research*, 117, D04304. <https://doi.org/10.1029/2011JD016360>
- Ren, X., Hall, D. L., Vinciguerra, T., Benish, S. E., Stratton, P. R., Ahn, D., et al. (2018). Retraction: Methane emissions from the Marcellus Shale in southwestern Pennsylvania and northern West Virginia based on airborne measurements. *Journal of Geophysical Research: Atmospheres*, 123, 1478–1478. <https://doi.org/10.1002/jgrd.54397>
- Saide, P., Carmichael, G., Spak, S., Minnis, P., & Ayers, J. (2012). Improving aerosol distributions below clouds by assimilating satellite-retrieved cloud droplet number. *Proceedings of the National Academy of Sciences of the United States of America*, 109(30), 11,939–11,943. <https://doi.org/10.1073/pnas.1205877109>
- Saide, P., Peterson, D. A., da Silva, A., Anderson, B., Ziemba, L. D., Diskin, G., et al. (2015). Revealing important nocturnal and day-to-day variations in fire smoke emissions through a multiplatform inversion. *Geophysical Research Letters*, 42, 3609–3618. <https://doi.org/10.1002/2015GL063737>
- Schwietzke, S., Pétron, G., Conley, S., Pickering, C., Mielke-Maday, I., Dlugokencky, E. J., et al. (2017). Improved mechanistic understanding of natural gas methane emissions from spatially resolved aircraft measurements. *Environmental Science & Technology*, 51(12), 7286–7294. <https://doi.org/10.1021/acs.est.7b01810>
- Sheng, J.-X., Jacob, D. J., Turner, A. J., Maasakkers, J. D., Sulprizio, M. P., Bloom, A. A., et al. (2018). High-resolution inversion of methane emissions in the southeast US using SEAC4RS aircraft observations of atmospheric methane: Anthropogenic and wetland sources. *Atmospheric Chemistry and Physics*, 18(9), 6483–6491. <https://doi.org/10.5194/acp-18-6483-2018>
- Tian, Y., Huffman, G. J., Adler, R. F., Tang, L., Sapiano, M., Maggioni, V., & Wu, H. (2013). Modeling errors in daily precipitation measurements: Additive or multiplicative? *Geophysical Research Letters*, 40, 2060–2065. <https://doi.org/10.1002/grl.50320>
- Turner, A. J., Jacob, D. J., Wecht, K. J., Maasakkers, J. D., Lundgren, E., Andrews, A. E., et al. (2015). Estimating global and North American methane emissions with high spatial resolution using GOSAT satellite data. *Atmospheric Chemistry and Physics*, 15(12), 7049–7069. <https://doi.org/10.5194/acp-15-7049-2015>
- United Nations Framework Convention on Climate Change (2016). INDCs as communicated by parties, available at: <http://www4.unfccc.int/Submissions/INDC/Submission%20Pages/submissions.aspx> (last access: 21 June 2018)
- Vaughn, T. L., Bell, C. S., Pickering, C. K., Schwietzke, S., Heath, G. A., Pétron, G., et al. (2018). Temporal variability largely explains top-down/bottom-up difference in methane emission estimates from a natural gas production region. *Proceedings of the National Academy of Sciences of the United States of America*, 115(46), 11,712–11,717. <https://doi.org/10.1073/pnas.1805687115>
- Warneke, C., Trainer, M., de Gouw, J. A., Parrish, D. D., Fahey, D. W., Ravishankara, A. R., et al. (2016). Instrumentation and measurement strategy for the NOAA SENEX aircraft campaign as part of the southeast atmosphere study 2013. *Atmospheric Measurement Techniques*, 9(7), 3063–3093. <https://doi.org/10.5194/amt-9-3063-2016>
- Wecht, K. J., Jacob, D. J., Frankenberg, C., Jiang, Z., & Blake, D. R. (2014). Mapping of North American methane emissions with high spatial resolution by inversion of SCIAMACHY satellite data. *Journal of Geophysical Research: Atmospheres*, 119, 7741–7756. <https://doi.org/10.1002/2014JD021551>
- Yuan, B., Kaser, L., Karl, T., Graus, M., Peischl, J., Campos, T. L., et al. (2015). Airborne flux measurements of methane and volatile organic compounds over the Haynesville and Marcellus shale gas production regions. *Journal of Geophysical Research: Atmospheres*, 120, 6271–6289. <https://doi.org/10.1002/2015JD023242>